Engineering of NEMO as calcium indicators with ultra-high dynamics and sensitivity

Jia Li[*1], Ziwei Shang[*2], Jia-Hui Chen[*3], Wenjia Gu[*1], Li Yao[*2], Xin Yang[4], Xiaowen Sun[2], Liuqing Wang[1], Tianlu Wang[5], Siyao Liu[5], Jiajing Li[1], Tingting Hou[6], Dajun Xing[2], Donald L. Gill[7], Jiejie Li[1], Shi-Qiang Wang[6], Lijuan Hou[4], Yubin Zhou[#5,8], Ai-Hui Tang[#3,9], Xiaohui Zhang[#2], Youjun Wang[#1,10]

[1] Beijing Key Laboratory of Gene Resource and Molecular Development, College of Life Sciences, Beijing Normal University, Beijing, 100875, China.

[2] State Key Laboratory of Cognitive Neuroscience & Learning, IDG/McGovern Institute for Brain Research, Beijing Normal University, Beijing, 100875, China. Email: xhzhang@bnu.edu.cn

[3] Hefei National Research Center for Physical Sciences at the Microscale, CAS Key Laboratory of Brain Function and Disease, and Ministry of Education Key Laboratory for Membrane-less Organelles & Cellular Dynamics, Division of Life Sciences and Medicine, University of Science and Technology of China, Hefei 230026, China. Email: tangah@ustc.edu.cn

[4] Exercise physiology and Neurobiology Lab, College of P.E. and Sports, Beijing Normal University, Beijing, 100875, China.

[5] Institute of Biosciences and Technology, Texas A&M University, Houston, TX, 77030, USA. Email: yubinzhou@tamu.edu

[6] State Key Laboratory of Membrane Biology, College of Life Sciences, Peking University, Beijing 100871, China

[7] Department of Cellular and Molecular Physiology, Pennsylvania State University College of Medicine, Hershey, Pennsylvania 17033

[8] Department of Translational Medical Sciences, School of Medicine, Texas A&M University, Houston, TX, 77030

[9] Institute of Artificial Intelligence, Hefei Comprehensive National Science Center, Hefei 230026, China

[10] Key Laboratory of Cell Proliferation and Regulation Biology, Ministry of Education, College of Life Sciences, Beijing Normal University, Beijing, 100875, China. Email: wyoujun@bnu.edu.cn

[*] These authors contributed equally to this work

[#] Corresponding authors

Abstract

Genetically-encoded calcium indicators (GECI) are indispensable tools for real-time monitoring of intracellular calcium signals and cellular activities in living organisms. Current GECIs face the challenge of sub-optimal peak signal-to-baseline-ratio (SBR) with limited resolution for reporting subtle calcium transients. We report herein the development of a suite of calcium sensors, designated NEMO, with fast kinetics and ultra-wide dynamic ranges (>200-fold). NEMO indicators report Ca^{2+} transients with peak SBRs ~20-fold larger than the top-of-the-range GCaMP series. NEMO sensors further enable the quantification of absolution calcium concentration with ratiometric or photochromic imaging. Compared to GCaMPs, NEMOs could detect single action potentials in neurons with a peak SBR two times higher and a median peak SBR four times larger *in vivo*, thereby outperforming most existing state-of-the-art GECIs. Given their ultra-high sensitivity and resolution to report intracellular Ca^{2+} signals, NEMO sensors may find broad applications in monitoring neuronal activities and other Ca^{2+}-modulated physiological processes in both mammals and plants.

Calcium ions (Ca^{2+}) are messengers essential for life and death, mediating responses ranging from neurotransmitter release, muscle contraction, to gene expression. The information is encoded in transient three-dimensional changes of Ca^{2+} concentration in space, time, and amplitude [1]. Genetically-encoded Ca^{2+} indicators (GECI) are indispensable tools for real-time monitoring of Ca^{2+} signals and cellular activities, such as neuronal activation [2]. The signal-to-baseline ratio (SBR; $\Delta F/F_0$), defined as the ratio of the absolute fluorescence (F) changes ($F-F_0$, or ΔF) over the basal fluorescence (F_0), is a key parameter used to gauge the performance of mono-colored GECIs [3]. Tremendous efforts have been devoted to generate GECIs with faster kinetics (e.g., jGCaMP8 series [4]), but progress toward increased maximal fluorescence change has remained relatively lagging since the development of GECO and GCaMP6 series approximately ten years ago [5,6].

With a Ca^{2+}-sensing module installed within one fluorescent protein (FP), single-FP-based indicators use Ca^{2+}-dependent fluorescence changes to report Ca^{2+} transients. Calmodulin (CaM) together with its target peptide (such as RS20 or M13) is among the most commonly-used Ca^{2+} sensing modules. Two strategies have been applied to link CaM-M13 with FP: (i) GCaMP-like design [6] to install CaM and M13 to the C- and N-termini of a FP, as exemplified by circularly permuted enhanced green FP (cpEGFP); and (ii) NCaMP7-like strategy [7] to insert CaM-M13 into the middle of a FP [8]. Over the past 20 years, modifications within the linkers or interaction interfaces among CaM, M13 and FP were proven successful strategies to improve the sensitivity, speed and dynamics of GCaMP variants [4,6,9]. Nevertheless, further improvements in their dynamic ranges, nevertheless, are restricted by the brightness of EGFP. While NCaMP7 or mNG-GECO[10] was built upon the brightest monomeric green FP, mNeonGreen (mNG) [11], they exhibited a relatively small *in cellulo* dynamic range [7]. By combining the advantages of both the GCaMP and NCaMP7 series, we set out to develop substantially improved GECIs with fast speed and ultra-high dynamic ranges building upon mNG.

Engineering of mNeonGreen-based calcium indicators (NEMO)

Single-FP-based indicators share some structural similarities at the sensing module insertion sites [8], with most GECI constructs using CaM-M13 as the Ca^{2+} sensing module [12]. We reasoned that

strategies for designing and optimizing CaM-based indicators might be transferable in principle among GECIs. We thus created a series of constructs mostly by applying known GECI design strategies toward mNG, and screened their performance in HEK293 cells (**Fig. 1A–C**, and **Supplementary Tables 1-2**).

We first evaluated the basal fluorescence (F_0) and the ratio between maximal (F_{max}) and minimal (F_{min}) fluorescence, or the dynamic range (F_{max}/ F_{min}), of mNG-based constructs. To allow measurements of F_{min}, the endoplasmic reticulum (ER) Ca^{2+} store in mammalian cells was depleted by incubating the cells in a Ca^{2+}-free buffer containing 300 μM EGTA, 2.5 μM ionomycin (iono) and 1 μM thapsigargin (TG) for 10 min. Ionomycin is an ionophore and TG is an inhibitor of the sarcoplasmic/endoplasmic reticulum Ca^{2+} ATPase, both of which serve as inducers of passive ER store depletion. Following this, a high amount of Ca^{2+} (100 mM) was added to the culture medium to induce F_{max} via store-operated Ca^{2+} entry (SOCE) (**Fig. 1B-C**). Time-lapsed imaging was used to monitor store depletion-induced changes in cytosolic Ca^{2+} concentrations by using NCaMP7 and GCaMP6m as the references (**Fig. 1B**). Top candidates (**Fig. 1C**) were identified based on both the F_0 and the dynamic range (F_{max}/F_{min}) values (**Fig. 1D**). We found that the GCaMP-like design [6] did not work out with mNG (**Supplementary Table 1**), while NCaMP7-like [7] variants (**Fig. 1A**) showed improved dynamics and speed (**Supplementary Table 2**). Among all the variants, we identified five best-performing constructs and named them as members of the mNeonGreen-based Calcium indicator (NEMO) family, including the medium (NEMOm), high contrast (NEMOc), fast (NEMOf), bright (NEMOb) and sensitive (NEMOs) versions (**Fig. 1D**, **Supplementary Fig. 1 and 2A**). We then analyzed their physiochemical and photonic properties and further explored possible applications under different physiological scenarios.

Ex vivo characterization of NEMO sensors

The overall *in cellulo* dynamic range of NEMO sensors seemed to be superior to that of top-of-the-range GECI proteins tested side-by-side. Compared with NCaMP7, NEMOs and NEMOb contain an extra N-terminal linker (L1) and a single amino acid substitution (M324I) in the linker (L4) between M13 and mNG (**Fig. 1A**). The dynamic ranges of NEMOs or NEMOb (102.3 ± 4.0 or 128.8

± 3.1, respectively) were found to be at least 4.5-fold higher than that of GCaMP6m or NCaMP7 (22.9 ± 0.3 and 15.8 ± 0.5, respectively; **Fig. 1D**). In addition to the M324I mutation, NEMOm and NEMOc possess additional modifications in the linker domain between CaM and M13 (**Fig. 1A**). As a result, dynamic ranges of these two indicators were further increased to 240.7 ± 7.6 and 422.2 ± 15.3, respectively, which were 9.5 to 25.7-fold higher than those of GCaMP6m or NCaMP7 (**Fig. 1D,** and **Supplementary video 1**). To the best of our knowledge, NEMO indicators represent a class of GECI sensors with an exceptional *in cellulo* dynamic range of over 100-fold.

To characterize Ca^{2+}-dependent properties of NEMO indicators more quantitatively, we performed *in vitro* Ca^{2+} titration experiments using recombinant NEMO proteins purified from bacteria. NEMOc, NEMOf, and NEMOs showed dynamic ranges of 182, 128, and 100-fold, respectively (**Fig. 1E**). Although brightest in the basal fluorescence among all NEMO variants, NEMOb showed a 66-fold change in the dynamic range, prompting us to focus on the other four variants for further characterization. Even though the Ca^{2+} binding affinity of NEMOs or NEMOm (155.8 ± 3.8 nM and 248.4 ± 3.7 nM, respectively) remained comparable to that of GCaMP6m (206.4 ± 5 nM), the *in vitro* dynamic range was 3.2 to 5.6-fold higher than that of GCaMP6m (**Fig. 1E**). Hence, the high *in cellulo* dynamic range of NEMO sensors does not seem to be related to their Ca^{2+}-binding affinities.

We next examined the basal fluorescence of NEMO sensors in HEK293 cells. We used a P2A-based bicistronic vector to drive the co-expression of mKate (as an expression marker) and GECIs at a near 1:1 ratio. The resting GECI brightness was indicated by the fluorescence ratio of GECI and mKate (**Fig. 1F**). Consistent with their lower Ca^{2+} binding affinities, normalized basal brightness of all NEMO sensors was much lower than that of NCaMP7, and the brightness of NEMOc or NEMOf was only approximately 0.25-0.5 of GCaMP6m. This finding indicates that the lower basal fluorescence of NEMO variants might contribute to the observed large dynamic range of NEMO indicators, in particular for NEMOc and NEMOf. However, even though the dynamic ranges of NEMOm, NEMOs and NEMOb were over 5-fold higher than that of GCaMP6m, their basal fluorescence was either similar to or brighter than that of GCaMP6m (**Fig. 1D, 1F**). Hence, high dynamic ranges for these three indicators could be attributed to their maximal brightness being larger than that of GCaMP6m as well. In consonance with this notion, NEMO-expressing cells with

comparable basal fluorescence to those expressing GCaMP6m still exhibited larger dynamics (**Fig. 1G**). Taken together, these results establish NEMO indicators as a class of GECIs with extraordinarily large Ca^{2+}-dependent changes in fluorescence.

Using NEMOc as an example, we next set out to decipher the mechanisms underlying the superior dynamic range of NEMO sensors. In GECI proteins, such as NCaMP7 [7] and most sensors from the GECO [13] and GCaMP series [14], fluorophores exist in two configurations: an anionic state and a neutral state. The Ca^{2+}-induced brightening of GECI fluorescence is caused by increasing both the proportion and molecular brightness of anionic form [7 13 14]. Similarly, the fluorophore of NEMOc adopted an anionic state, with a peak absorption at 509 nm, and a neutral state, with the maximal absorption at 403 nm (**Supplementary Fig. 2B**). Analysis of the pH dependence of absorption spectra revealed that Ca^{2+}-induced increase in the proportion of anionic NEMOc was similar to that of NCaMP7, but smaller than that of GCaMP6m (**Supplementary Fig. 2C–E**, and **Supplementary Table 4**). The Ca^{2+}-induced brightening of the anionic fluorophore of NEMOc (292.1-fold increase) turned out to be 5–13 times larger than that of NCaMP7 or GCaMP6m (49- and 21.3-fold increase, respectively) (**Supplementary Table 4**). However, the increase in the dynamic range was mostly associated with the considerably dimmer anionic fluorophore of NEMOc (0.22 ± 0.01 $mM^{-1}cm^{-1}$) in the absence of Ca^{2+}, which was approximately one-sixth that of NCaMP7 (1.34 ± 0.06 $mM^{-1}cm^{-1}$) and one-fifth that of GCaMP6m (1.11 ± 0.13 $mM^{-1}cm^{-1}$). Compared to GCaMP6m, the high dynamic range of NEMOc was also a result of increased brightness of Ca^{2+}-saturated anionic NEMOc (64.26 ± 2.67 $mM^{-1}cm^{-1}$), approximately three times that of GCaMP6m (23.66 ± 1.22 $mM^{-1}cm^{-1}$). Moreover, we examined the *in vitro* normalized two-photon action cross-sections of NEMOc and *in cellulo* dynamic range of NEMOs under two-photon excitation when expressed in HEK293 cells. The properties and performance of NEMO sensors relative to GCaMP6m or NCaMP7 remained largely similar to those observed with one-photon excitation (**Supplementary Fig. 3A–B**). Overall, these findings indicate that the superior dynamic range of NEMO indicators can be largely ascribed to the Ca^{2+}-dependent fold-of-increase in the molecular brightness of the anionic fluorophores in NEMO variants.

Some NEMO indicators, however, showed lower basal fluorescence (**Fig. 1F**). To examine whether it is possible to compensate weaker NEMO fluorescence with stronger illumination, we

measured the photostability of NEMO sensors. mNG as the template of NEMO is more prone to photobleaching than EGFP, the FP template used in GCaMP6m (**Supplementary Fig. 4A**) [11]. However, engineered mNG-based NEMOm showed better photostability than GCaMP6m or mNG (**Supplementary Fig. 4A,** top left two panels). It endured nearly 40 times (1.52 mW) higher illumination than GCaMP6m (0.04 mW), and showed no apparent photobleaching. The stronger illumination (from 0.04 mW to 1.52 mW) could potentially enhance the basal fluorescence of NEMOm sensor by over 60-fold (**Supplementary Fig. 4A,** top right panel), greatly broadening the applicability of NEMO sensors in scenarios requiring stronger light illumination, such as monitoring Ca^{2+} signals *in vivo* within subcellular compartments with dim NEMOf indicator. Collectively, these results established NEMO variants as photostable biosensors with ultra-large dynamic ranges.

Performance of NEMO sensors in non-excitable cells

We next moved on to compare the ability of NEMO sensors to report receptor-mediated signals with frequently-used GECI sensors, including GCaMP6m, NCaMP7 and the most recently-developed jGCaMP8f [4]. We used a submaximal dose of carbachol (CCh, 10 μM), an agonist of muscarinic acetylcholinergic receptors, to induce Ca^{2+} transients and subsequent Ca^{2+} oscillation in HEK293 cells transfected with different GECIs. Peak signal-to-baseline (SBR, $\Delta F/F_0$) values of NEMOb (26.7 ± 2.2) and NEMOs (32.1 ± 2.2) were at least three times higher than those of GCaMP6m (7.5 ± 0.4), jGCaMP8f (5.1 ± 0.1), and NCaMP7 (5.5 ± 0.3) (**Fig. 2A, Supplementary Fig. 4B, C**). The SBRs of NEMOm (101.9 ± 6.6), NEMOc (112.0 ± 9.8) and NEMOf (194.3 ± 7.7) were 13-25 times higher than that of GCaMP6m. Similarly, the performance of NEMO sensors in reporting CCh-induced Ca^{2+} oscillations was found to be superior over jGCaMP8f and NCaMP7 under the same imaging conditions (**Fig. 2A, Supplementary Fig. 4B-C,** and **Supplementary Video 2**).

We further examined the performance of NEMO sensors in detecting weak Ca^{2+} signals. In the first test, we monitored TG-induced Ca^{2+} release and the SOCE response in mammalian cells. In this scenario, the peak SBR values of NEMO sensors were found to be at least 5 times higher than that of NCaMP7 (**Fig. 2B,** and **Supplementary Fig. 4D**). We then tested their capability to monitor Ca^{2+} transients generated via activation of the *Bombyx mori* gustatory receptor (BmGr-9), which is

known to be much smaller than SOCE in terms of the Ca^{2+} signal amplitude [15]. Similarly, the responses of NEMO sensors were much stronger than that of GCaMP6s (**Fig. 2C**). Taken together, intensiometric changes of NEMO sensors in response to the investigated Ca^{2+} signals in non-excitable cells are remarkably larger than those of other GECI sensors tested in our side-by-side comparisons.

We next examined whether the larger dynamic range of NEMO sensors could enable more sensitive detection of Ca^{2+} signals, which would otherwise appear to have a similar magnitude of response due to the smaller dynamic range using existing GECIs. We compared the performance of NEMO sensors with GECIs bearing comparable Ca^{2+}-binding affinities in response to small or large Ca^{2+} signals. We first tested the idea by resorting to an optogenetic tool, Opto-CRAC, which enables the stepwise induction of increased Ca^{2+} influx due to graded activation of endogenous ORAI Ca^{2+} channels by varying the photo-activation duration[16-18]. Opto-CRAC was subsequently co-expressed in HeLa cells along with NEMOm or GCaMP6m, respectively, for side-by-side comparison of photo-induced Ca^{2+} signals. Compared to GCaMP6m that poorly reported light-induced Ca^{2+} influx in small magnitudes, the NEMOm signals were significantly larger, with the amplitudes of NEMOm response showing a stepwise increase in response to prolonged photo-stimulation from 100 ms, 300 ms to 1000 ms (**Fig. S5A**, and **Supplementary Video 3**). Second, we compared the SOCE responses of HEK293 cells when exposed to increasing extracellular Ca^{2+} concentrations. NEMOm or NEMOs could discriminate more external Ca^{2+} gradients than GCaMP6m or NCaMP7 did (**Fig. S5B-C**). Moreover, the signal-to-noise ratios (SNRs) of NEMOm and NEMOs were significantly higher than their corresponding counterparts, which may also contribute to their better resolvability over the amplitudes of Ca^{2+} signals (**Fig. S5D-E**).

One major drawback of intensiometric Ca^{2+} sensors is that they could not be employed to directly report Ca^{2+} concentration. We thus asked whether NEMO sensors bear some photochemical features to allow the measurements of absolute Ca^{2+} concentrations. To this end, we first explored the use of NEMO as ratiometric sensors. The apoNEMO variant showed a small but appreciable excitation peak at 403 nm (**Supplementary Fig. 2A**). Furthermore, the fluorescence of apoNEMOs excited by 405 nm light (F_{405}) was brighter than its Ca^{2+}-bound form. *In vitro* Ca^{2+} titration revealed that the F_{405} response of NEMOs reduced as a function of increasing Ca^{2+} concentration with an

apparent K_d of 234 ± 15 nM, as opposed to the Ca^{2+}-induced enhancement of NEMOs fluorescence excited by 490 nm light (F_{490}) (**Supplementary Fig. 6A**). Consequently, the dynamic range indicated by the F_{490}/F_{405} ratio was 3.4-fold higher than that obtained with F_{490} only (**Supplementary Fig. 6B**). A similar trend was also visualized in HEK293 cells expressing NEMOs, with the ratiometric dynamic ranges significantly larger than intensiometric ones (**Fig. 2D,** and **Supplementary Fig. 6C-D**).

While performing ratiometric recordings, we noticed that the UV illumination approximately doubled the fluorescence intensity of NEMO sensors under low Ca^{2+} conditions, indicating the existence of a photochromic effect [19] (**Supplementary Fig. 6E**). We thus asked whether NEMO indicators could also report Ca^{2+} concentration with a newly-developed intermittent photochromism-enabled absolute quantification (iPEAQ) method [19], which allows measurements of Ca^{2+} levels using photochromism contrast independent on GECI concentrations and the intensity of excitation light. Indeed, we found that NEMOf and NEMOs exhibited photochromic characteristics. Brief 405 nm UV illumination superimposed on 488 nm light could increase NEMOf fluorescence in an inversely Ca^{2+} dependent manner, with the peak fluorescence named as F_0. After switching off the UV light, NEMOf quickly relaxed back to its basal state, or termed as the minimal fluorescence (F_{end}) (**Supplementary Fig. 6F**). One such photochromic cycle would allow the calculation of photochromism contrast, defined as $((F_0 - F_{end}) / F_0)_{hv}$. We then quantified Ca^{2+} release induced by submaximal stimulation of muscarinic acetylcholinergic receptor with 10 μM CCh by taking the iPEAQ approach. Briefly, based on a Ca^{2+}-titration curve of photochromism contrast (**Supplementary Fig. 6G**, left), we converted the measured rest photochromism contrast of a NEMOs-expressing cell to basal Ca^{2+} concentration. With this calculated resting Ca^{2+} level and the Ca^{2+}-NEMOs fluorescence response curve (**Supplementary Fig. 6G**, right), the NEMOs fluorescence response of each cell could then be calculated as changes in the absolute Ca^{2+} concentrations (**Fig. 2E**). Collectively, NEMO sensors can be used as ratiometric or photochromic indicators [19], not only reporting Ca^{2+} signals with an improved resolution of amplitude but also capable of indicating absolute Ca^{2+} levels.

Assessing NEMO sensors in neurons and in planta

We next examined the responses of NEMO sensors in cultured neurons dissociated from fetal rat hippocampus. We excited neurons that expressed different GECI constructs using electrical field stimulation, and measured the corresponding changes in fluorescence signals of the sensors with the excitation/emission setup best tailored for GCaMP (**Fig. 3**). We observed that all NEMO sensors were sensitive enough to detect Ca^{2+} signals elicited by even a single action potential (AP) (**Fig. 3A**), with peak SBR approximately twice as high as GCaMP6s (0.12 ± 0.01) or GCaMP6f (0.11 ± 0.03). Consistent with the *in vitro* analysis demonstrating that the K_{off} of NEMOf was higher than that of GCaMP6f (**Supplementary Table 3**), NEMOf was fast enough to discriminate neuronal responses induced by electrical field stimulation with a frequency up to 5 Hz (**Fig. 3B**). These observations indicate that NEMO sensors perform similarly or better than the existing EGFP-based sensors in terms of single-AP detection sensitivity and response time.

Similar to what we observed in non-excitable cells, the ultra-high dynamic range of NEMO sensors enabled high-resolution detection of Ca^{2+} signals of various amplitudes. In response to a 5 Hz field stimulation, the peak amplitude of NEMOf response ($\Delta F/F_0$, 2.9 ± 0.5) was approximately three times that of GCaMP6f, placing NEMOf among the most sensitive and fast GECIs that include XCaMP[20], jGCaMP7[9], or jGCaMP8 series[4]. As the stimulus frequency increased, the difference between peak NEMOf and GCaMP6f responses became more pronounced. For example, NEMOf response induced by 10 Hz simulation was approximately 5 times that of GCaMP6f (**Fig. 3C**), while the peak NEMOf signal in response to 180 Hz stimulation was 22.7 times that of GCaMP6f (**Fig. 3D**). Over the entire range of stimulus intensities tested, the responses of all NEMO sensors were significantly stronger than those of GCaMP6s, GCaMP6f, and jGCaMP8f (**Fig. 3D**), often with their SNRs significantly larger than their counterparts (**Supplementary Fig. 7A**). The NEMO sensors also reported the frequency of the stimulus in a fairly linear manner, with no apparent saturation even up to 180 Hz (**Fig. 3E**), indicating that NEMO sensors are suitable for resolving neuronal Ca^{2+} dynamics in response to the full spectrum of activities under physiological conditions.

We further tested NEMO sensors in cortical neurons in acutely-prepared mouse brain slices combining two-photon laser Ca^{2+} imaging and whole-cell electrophysiological recording. We transfected layer 2/3 neurons in the primary visual cortex (V1) with adeno-associated virus (AAV), in which GECI expression was driven by the human synapsin I promoter, a neuron-specific promoter

(AAV-hsyn1-GECI constructs), through a stereotaxic injection. Three weeks later, cytoplasmic fluorescence was detectable in the majority of layer 2/3 neurons. AP was elicited by intracellular injection of a current pulse train via the recording micropipette, and the corresponding signals of GECI sensors were recorded and compared (**Supplementary Fig. 7B**, left panel). Under a whole-cell patch clamp condition, the intracellular environment could be perturbed and the GECI signal was diluted [20]. Despite of this caveat, the responses of all NEMO sensors induced by AP occurring at 50 Hz or higher frequencies were significantly higher than those of GCaMP6s or GCaMP6f (**Supplementary Fig. 7B**, middle panel). Consistent with data obtained using dissociated neurons, the response of NEMO sensors was significantly more pronounced under most tested conditions, with NEMOf exhibiting the fastest kinetics (**Supplementary Fig. 7B**, middle and right panel). Of note, most fast GECI sensors developed to date (e.g., RCaMP2[21], jRGECO1a[22], XCaMP-Gf[20], and jGCaMP8f[4]) display rather limited dynamic ranges. By contrast, NEMOf expressed in both non-excitable and excitable cells shows fast and ultra-high dynamic range, making it an ideal tool to decode fast and highly dynamic Ca^{2+} signals in living cells and tissues.

To generalize the application of NEMO sensors beyond mammals, we tested the usability of NEMO sensors in detecting subcellular Ca^{2+} signals in the leaves of *Arabidopsis thaliana*. This was made possible by fusing NEMOm to plasmodesmata-localized protein 1 as a marker for plasmodesmata, a unique structure between plant cells with a diameter about 30~60 nm [23]. Our super-resolution imaging results showed that NEMOm could readily report the existence of Ca^{2+} oscillations near the plasmodesmata (**Supplementary Fig. 8E, Supplementary Video 4)**. This finding firmly establishes the feasibility of applying NEMO sensors *in planta*.

In vivo **performance of NEMO sensors evaluated in rodent brains**

We next tested the performance of NEMO sensors in neurons of mouse primary visual cortex (V1) *in vivo* using two-photon laser microscopy (**Fig. 4A**). Three weeks after transfection with AAV-hsyn1-GECI constructs, we presented drifting grating stimulus to one eye of anesthetized mice to evoke spiking activity of layer 2/3 neurons in the contralateral V1[24], and then monitored corresponding fluorescence signals of GECI sensors in these neurons evoked by the visual stimulus.

To ensure direct comparison with GCaMP6 sensors, we used 920 nm light, an excitation wavelength optimized for GCaMP but less ideal for NEMO (980 nm) to excite the GECIs. All the tested indicators accurately reported differential changes in response to different orientations or directions of visual stimuli (**Fig. 4B,** and **Supplementary Fig. 7C-D**). Consistent with *in vitro* characterization, NEMOm was relatively slow, with half decay time similar to GCaMP6s (1.36 ± 0.08 s). The half decay time of NEMOs was 1.17 ± 0.03 s, slightly shorter than that of GCaMP6s. NEMOf was the fastest among all NEMO variants, with the half decay time (409 ± 54 ms) comparable to GCaMP6f (482 ± 48 ms) (**Supplementary Fig. 7E**).

We then moved on to compare the sensitivity of GECIs *in vivo*. When examined by the fraction of responsive cells (**Supplementary Fig. 7F**), no significant difference between NEMO variants and the corresponding GCaMP6 indicators was detected. However, considering the peak fluorescence response, the cumulative distribution of peak $\Delta F/F_0$ of NEMOm and NEMOs was substantially right-shifted relative to the GCaMP6 signal (**Fig. 4C**), indicating that NEMOm and NEMOs are more responsive. The median response of NEMOs ($\Delta F/F_0$ =3) was over four and seven times stronger than that of GCaMP6s ($\Delta F/F_0$ = 0.73) and GcaMP6f ($\Delta F/F_0$ = 0.44), respectively. The visual-stimuli-induced response reported by NEMOs was much larger than existing values reported by sensitive GECIs such as jRGECO1a [22], jYCaMP1s [25], jGCaMP7s [9] or jGCaMP8s [4]. In parallel, the median response of NEMOf ($\Delta F/F_0$ = 0.80) was significantly larger than that of GCaMP6f ($\Delta F/F_0$ = 0.44) (right panel in **Fig. 4B** versus **Supplementary Fig. 7C**, left panel), as well as those reported by the known fastest GECIs, such as R-CaMP2 [21], jRGECO1a [22], jGCaMP7f [9] and jGCaMP8f [4].

In addition, NEMOs showed appreciably better SNR (**Supplementary Fig. 7G**) and good basal fluorescence in the mouse V1 that was comparable to GCaMP6s even under excitation conditions optimized for GCaMP (**Supplementary Fig. 8A-B**). Probably due to its weak fluorescence, NEMOf signal obtained with GCaMP set up showed similar SNR to GCaMP6f (**Supplementary Fig. 7G**). Since the basal NEMOm fluorescence approximately doubled by switching from GCaMP excitation (920 nm) to a NEMO setup (980 nm) (**Supplementary Fig. 8C**), we thus collected NEMOf signals with 980 nm light. The results showed that NEMOf under optimized illumination retained its large SBR (**Supplementary Fig. 8D**, left panel), and the SNR of NEMOf was significantly better than

that of GCaMP6f or NEMOf with 920nm excitation (**Supplementary Fig. 8D**, right panel). Since GCaMP6s and NCaMP7 were reported to have similar *in vivo* SNR [7], it is likely that optimally-excited NEMOs (i.e., at 980 nm) may exhibit a better SNR than NCaMP7.

Lastly, we recorded the fluorescence response of NEMOs in neurons deeply buried in the mouse brain using fiber photometry and settings optimized for GCaMP recordings [26]. Neurons within the corpus striatum were infected with AAV-hsyn1-NEMOs or AAV-hsyn1-GCaMP6f. Two weeks later, the GECI fluorescence signals excited by 410 nm (F_{410}) or 470 nm light (F_{470}) were collected, and Ca^{2+} responses within the neurons elicited by tail-pinching stimulus were evaluated using the F_{470}/F_{410} ratio (R) (**Fig. 4D**). Even though the near-UV light (410 nm) excitation reduced the dynamics of NEMO and the 470 nm light was not optimal for NEMOs excitation (**Supplementary Fig. 2A** and **Supplementary Fig. 6D**), the NEMOs-reported Ca^{2+} transients evoked by the sensory stimulus were still larger than GCaMP6f (**Fig. 4E**), with the median peak response of NEMOs being approximately 3 times that of GCaMP6f ($\Delta R/R_0$: 20.2 vs 6.5). Collectively, NEMOs and NEMOf are among the most sensitive GECI tools for *in vivo* monitoring of both slow and fast neural activities with a better SNR.

Conclusions

In the current study, we reported a series of GECIs with greatly improved photochemical properties. Unlike current state-of-the-art Ca^{2+} indicators that partially sacrifice the dynamic range for improved sensitivity and/or faster kinetics, NEMO variants are fast acting while still retaining ultra-high dynamic ranges to report Ca^{2+} signaling both *ex vivo* and *in vivo*. They are more versatile than the most popular GCaMP series, allowing simultaneous imaging with cyan fluorescence while exhibiting higher photostability that can endure substantially stronger illumination, thereby meeting the demand for varying basal fluorescence under different circumstances. Overall, the ultra-sensitive NEMO sensors may serve as the tool-of-choice for monitoring Ca^{2+} dynamics in both excitable and non-excitable mammalian cells, tissue, or *in vivo*, as well as *in planta*.

ACKNOWLEDGMENTS

This work was supported by the National Natural Science Foundation of China (91954205 to Y.W.; 32130043 and 32071025 to X-h. Z.; 31872759 to A.-H. T.; 31971095 to L.H.; and 32171033 to D. X., 91854209, 32230048 and 92254301 to S-Q. W, 92054101 and 32122013 to J. L.), National Science and Technology Innovation 2030 Grants (2022ZD0204900 to X-h. Z.; 2021ZD0202503 to A.-H. T.), the National Key Research and Development Program of China (2020YFA0112200 to A.-H. T.), and the Ministry of Science and Technology of China (2019YFA0802104 to Y.W.), the Welch Foundation (BE-1913-20220331 to YZ), and the China Postdoctoral Science Foundation (2021M703089 to J.C.).

Author contributions

YW, X-h Z, AT, LH, YZ supervised and coordinated the study. JL designed and generated all the plasmid constructs. JL and WG performed the *in vitro* assays. JL performed all fluorescence imaging in HEK cells, with help from WG and LW. TW and SL performed the optogenetic experiments. JC performed confocal imaging of dissociated neurons. TH performed confocal imaging of dissociated cardiac cells. LY performed two-photon Ca^{2+} imaging of whole-cell patched neurons in mouse brain slices. JL made the transgenetic *Arabidopsis thaliana* and carried out super resolution imaging of plasmodesmata. ZS performed *in vivo* two-photon Ca^{2+} imaging of visual cortical neurons in mice. XS monitored basal fluorescence of indicators in mice visual cortex. XY performed fiber photometry *in vivo*. JL, ZS, JC, WG, LW, LY, ZS, XY and XS analyzed data, with input from the other authors. DLG, SW, DX, and JL provided intellectual input to the manuscript. YZ, X-h Z and YW wrote the manuscript with inputs from all the other authors.

Conflicts of interests

All authors declare no conflicts of interests.

References

1 Berridge, M. J., Lipp, P. & Bootman, M. D. The versatility and universality of calcium signalling. *Nat Rev Mol Cell Biol* **1**, 11-21, doi:10.1038/35036035 (2000).

2 Lin, M. Z. & Schnitzer, M. J. Genetically encoded indicators of neuronal activity. *Nature*

neuroscience **19**, 1142-1153, doi:10.1038/nn.4359 (2016).

3 Perez Koldenkova, V. & Nagai, T. Genetically encoded Ca(2+) indicators: properties and evaluation. *Biochimica et biophysica acta* **1833**, 1787-1797, doi:10.1016/j.bbamcr.2013.01.011 (2013).

4 Y. Zhang, M. R., D. Bushey, J. Zheng, D. Reep, G. J. Broussard, A. Tsang, G. Tsegaye, , R. Patel, S. N., J. X. Lim, R. Zhang, M. B. Ahrens, G. C. Turner, S. S.-H. Wang, K. & Svoboda, W. K., E. R. Schreiter, J. P. Hasseman, I. Kolb, L. L. Looger. jGCaMP8 fast genetically encoded calcium indicators. doi:10.25378/janelia.13148243 (2020).

5 Zhao, Y. *et al.* An expanded palette of genetically encoded Ca(2)(+) indicators. *Science* **333**, 1888-1891, doi:10.1126/science.1208592 (2011).

6 Chen, T. W. *et al.* Ultrasensitive fluorescent proteins for imaging neuronal activity. *Nature* **499**, 295-300, doi:10.1038/nature12354 (2013).

7 Subach, O. M. *et al.* Novel Genetically Encoded Bright Positive Calcium Indicator NCaMP7 Based on the mNeonGreen Fluorescent Protein. *Int J Mol Sci* **21**, doi:10.3390/ijms21051644 (2020).

8 Nasu, Y., Shen, Y., Kramer, L. & Campbell, R. E. Structure- and mechanism-guided design of single fluorescent protein-based biosensors. *Nature chemical biology* **17**, 509-518, doi:10.1038/s41589-020-00718-x (2021).

9 Dana, H. *et al.* High-performance calcium sensors for imaging activity in neuronal populations and microcompartments. *Nat Methods* **16**, 649-657, doi:10.1038/s41592-019-0435-6 (2019).

10 Landon Zarowny, A. A., Virginia Rutten, Ilya Kolb, The GENIE Project, Ronak Patel, Hsin-Yi Huang, Yu-Fen Chang, Tiffany Phan, Richard Kanyo, Misha Ahrens, W. Ted Allison, Kaspar Podgorski, Robert E. Campbell. A bright and high-performance 1 genetically encoded Ca^{2+} indicator based on mNeonGreen fluorescent protein. *bioRxiv* (2020).

11 Shaner, N. C. *et al.* A bright monomeric green fluorescent protein derived from Branchiostoma lanceolatum. *Nat Methods* **10**, 407-409, doi:10.1038/nmeth.2413 (2013).

12 Horikawa, K. Recent progress in the development of genetically encoded Ca2+ indicators. *The journal of medical investigation : JMI* **62**, 24-28, doi:10.2152/jmi.62.24 (2015).

13 Molina, R. S. *et al.* Understanding the Fluorescence Change in Red Genetically Encoded Calcium Ion Indicators. *Biophysical journal* **116**, 1873-1886, doi:10.1016/j.bpj.2019.04.007 (2019).

14 Barnett, L. M., Hughes, T. E. & Drobizhev, M. Deciphering the molecular mechanism responsible for GCaMP6m's Ca2+-dependent change in fluorescence. *PLoS One* **12**, e0170934, doi:10.1371/journal.pone.0170934 (2017).

15 Sato, K., Tanaka, K. & Touhara, K. Sugar-regulated cation channel formed by an insect gustatory receptor. *Proceedings Of the National Academy Of Sciences Of the United States Of America* **108**, 11680-11685, doi:10.1073/pnas.1019622108 (2011).

16 He, L. *et al.* Near-infrared photoactivatable control of Ca(2+) signaling and optogenetic immunomodulation. *Elife* **4**, doi:10.7554/eLife.10024 (2015).

17 Ma, G. *et al.* Optogenetic toolkit for precise control of calcium signaling. *Cell Calcium* **64**, 36-46, doi:S0143-4160(16)30216-0 [pii]10.1016/j.ceca.2017.01.004 (2017).

18 Tan, P., He, L., Huang, Y. & Zhou, Y. Optophysiology: Illuminating cell physiology with optogenetics. *Physiological Reviews* **102**, 1263-1325, doi:10.1152/physrev.00021.2021

(2022).
19 Bierbuesse, F. *et al.* Absolute measurement of cellular activities using photochromic single-fluorophore biosensors and intermittent quantification. *Nature communications* **13**, 1850, doi:10.1038/s41467-022-29508-w (2022).
20 Inoue, M. *et al.* Rational Engineering of XCaMPs, a Multicolor GECI Suite for In Vivo Imaging of Complex Brain Circuit Dynamics. *Cell* **177**, 1346-1360.e1324, doi:10.1016/j.cell.2019.04.007 (2019).
21 Inoue, M. *et al.* Rational design of a high-affinity, fast, red calcium indicator R-CaMP2. *Nature methods* **12**, 64-70, doi:10.1038/nmeth.3185 (2015).
22 Dana, H. *et al.* Sensitive red protein calcium indicators for imaging neural activity. **5**, doi:10.7554/eLife.12727 (2016).
23 Thomas, C. L., Bayer, E. M., Ritzenthaler, C., Fernandez-Calvino, L. & Maule, A. J. Specific targeting of a plasmodesmal protein affecting cell-to-cell communication. *PLoS biology* **6**, e7, doi:10.1371/journal.pbio.0060007 (2008).
24 Niell, C. M. & Stryker, M. P. Highly selective receptive fields in mouse visual cortex. *The Journal of neuroscience : the official journal of the Society for Neuroscience* **28**, 7520-7536, doi:10.1523/JNEUROSCI.0623-08.2008 (2008).
25 Mohr, M. A. *et al.* jYCaMP: an optimized calcium indicator for two-photon imaging at fiber laser wavelengths. *Nature methods* **17**, 694-697, doi:10.1038/s41592-020-0835-7 (2020).
26 Cui, G. *et al.* Deep brain optical measurements of cell type-specific neural activity in behaving mice. *Nature protocols* **9**, 1213-1228, doi:10.1038/nprot.2014.080 (2014).

Figure Legends

Figure 1. Screening and *in vitro* characterization of NEMO indicators.

(A) NEMO sensors are generated by introducing amino acid substitutions in NCaMP7. Top panel, a diagram showing the design of NEMO variants; a table (middle panel) or NCaMP7 structure [7] (bottom panel) showing key amino acids substitutions introduced into NCaMP7 to generate NEMO variants.

(B–E) Screening of GCaMP and NCaMP7 variants in HEK293 cells. B) Ca^{2+} imaging-based screening. A typical trace from NCaMP7-expressing cells is shown. To avoid saturation of the camera, after recording the rest fluorescence (F_0) with regular exposure time (approximately 500 ms), time-series for variants with high dynamic range were recorded using one-tenth to one-fifth the exposure time. Afterwards, the fluorescence response curves of each cell were scaled up according to the corresponding F_0. After recording F_0, endoplasmic reticulum Ca^{2+} store was depleted using 2.5 μM ionomycin (iono) and 1 μM thapsigargin (TG). Then, the cells were incubated in an imaging solution containing 300 μM EGTA, to read minimal GECI fluorescence (F_{min}). Finally,

the cells were exposed to imaging solution containing 100 mM Ca^{2+} to obtain the maximal response (F_{max}) via store-operated Ca^{2+} entry. C) Representative traces of GCaMP6m and NCaMP7 (left), or selected NEMO sensors (right). D) Scatter plot of F_0–mean dynamic range (F_{max}/F_{min}) of the indicated GECIs. E) *In vitro* dose–response curves of NEMO sensors. Top, typical traces; Bottom, statistics (see **Supplemental Table 3** for details) (n=3 independent biological replicates; >17 cells per repeat).

(F) Basal brightness of NEMO, NCaMP7 or GCaMP sensors. To achieve better estimation of the basal fluorescence of GECIs (F_{GECI}), F_{GECI} of cells expressing mKate-P2A-GECI constructs were normalized against the fluorescence of mKate, an expression marker (F_{mKate}).

(G) F_0–dynamic range of individual cells expressing NEMO variants or GCaMP6m. To more accurately compare the performance of NEMO sensors with existing GECIs, the resting fluorescence of NEMO indicators in D) and G) were scaled with a factor F (calculated as F=(basal GECI ratio)/(rest GCaMP6m ratio)).

Figure 2. Performance of NEMO sensors in non-excitable mammalian cells.

(A) Typical Ca^{2+} oscillations in HEK293 cells induced by carbachol (CCh, 10 μM), as indicated by GCaMP6m, NCaMP7, and NEMO sensors. n=3 independent biological replicates, with at least 15 cells per repeat.

(B) Ca^{2+} release and store-operated Ca^{2+} entry (SOCE) responses induced by thapsigargin (TG). n=3 independent biological replicates, with at least 20 cells per repeat.

(C) Fructose-elicited response in cells co-expressing BmGr-9, an insect fructose receptor. Left, typical traces; right, statistics ($p < 0.0001$, unpaired Student's *t*-test, two-tailed). n=3 independent biological replicates, with at least 9 cells per repeat.

(D-E) Measurements of Ca^{2+} concentration with NEMO sensors. D) Ratiometric measurements with NEMOs. NEMOs transients in cells upon excitation at 488 nm or 405 nm, induced by 100 μM CCh. Left, typical NEMOs fluorescence response when excited at 488 nm or 405 nm. Right, representative intensiometric (black) or ratiometric (red, F_{488ex}/F_{405ex}) responses of the same set of cells shown on the left. n = 3 independent biological replicates, with at least 16 cells per repeat. E)

Intermittent photochromism-enabled absolute quantification (iPEAQ) of Ca^{2+} levels. Shown are fluorescence intensities (purple) and [Ca^{2+}] traces (green) of NEMOs-expressing cells in response to 10 μM CCh. In-cell calibration to determine the absolute Ca^{2+} concentration, or [Ca^{2+}], was shown in **Supplementary Fig. 4G**. n = 3 independent biological replicates, with at least 9 cells per repeat.

Figure 3. Electric field stimulation-induced NEMO responses in rat hippocampal neurons.

(A) Average Ca^{2+} responses reported by GECIs 1 Hz stimulation.

(B-C) Mean NEMOf and GCaMP6f transients induced by 5 Hz (B) or 10 Hz (C) stimulation.

(D) Mean GECI responses elicited by stimulation at varied frequencies. Inset, enlarged views of responses of reference GECI sensors (SBR magnified by 9 times).

(E) Statistics for data shown in panels A and D. Each GECI measurement set was analyzed from multiple dendrites of at least 10 neurons in three different primary hippocampal neuron cultures.

Figure 4. *In vivo* performance of NEMO sensors in monitoring neuronal activities in rodent brain.

(A–C) Fluorescence responses in the visual cortex of mice induced by a visual stimulus. A) Diagram showing the experimental setups for two-photon imaging of neurons in response to drift gratings. B) Typical response curves for GCaMP6s, NEMOs and NEMOf. C) Cumulative distribution of peak signal-to-baseline-ratio (SBR) transients of GECI sensors.

(D–F) Ratiometric responses of GCaMP6f and NEMOs in neurons of the mouse corpus striatum recorded by fiber photometry. D) Diagram of the experimental setup for fiber photometry recordings. E) Mean ratiometric responses elicited by pinch stimulation at the mouse tail tip. Left, mean traces; right, statistics ($p < 0.0001$, unpaired Student's *t*-test, two-tailed). NEMOs, data for 101 cells from 6 mice; GCaMP6f, data for 97 cells from 6 mice. F) Cumulative distribution of peak responses shown in E ($p = 1.6E-21$; Kolmogorov–Smirnov test).

Figure 1

A

	L1	CaM	L3	L4
NCaMP7	N/A	Q3-A15-M36	GGSGGGSSS	MYF
NEMOs	GITLGMDELYK	Q3-A15-M36	GGSGGGSSS	IYF
NEMOb	GGS	Q3-A15-M36	GGSGGGSSS	IYF
NEMOf	GGS	D3-E15-F36	GGGGS	IYF
NEMOc	N/A	Q3-A15-M36	GGGGS	IYF
NEMOm	GGS	Q3-A15-M36	GGSGGS	IYF

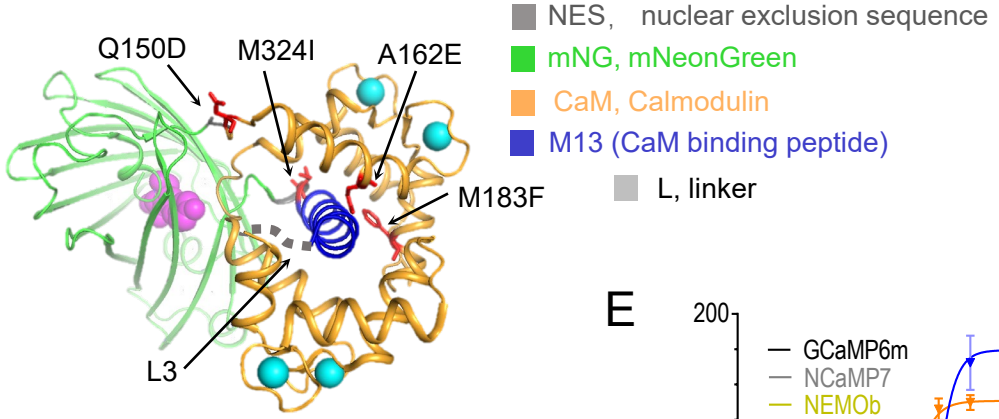

B

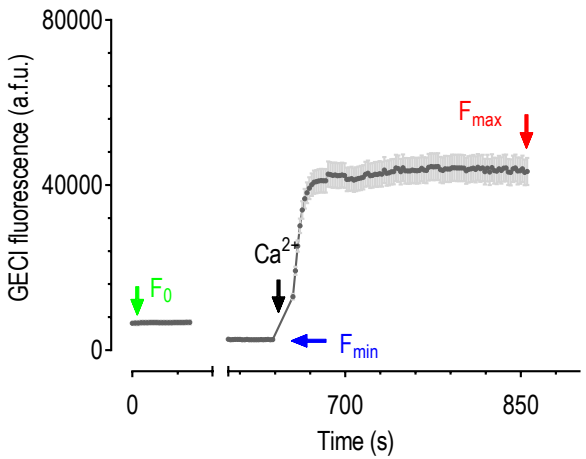

C

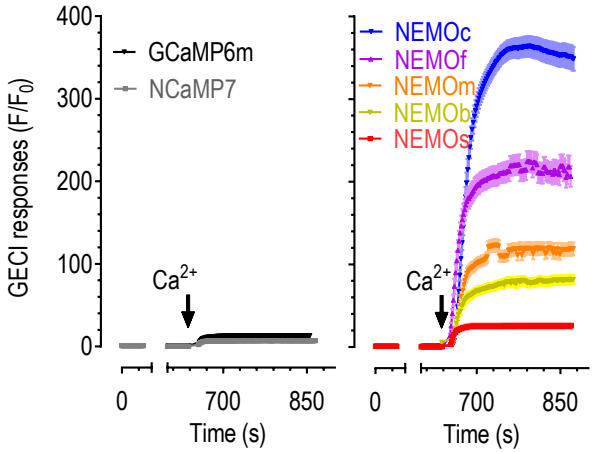

D

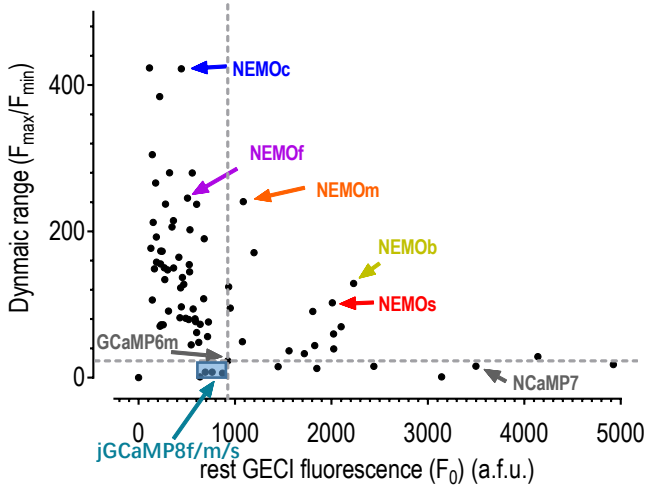

E

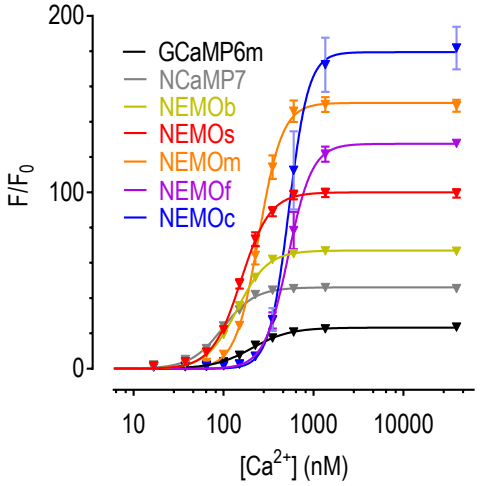

	K_d (nM)	$Hill_n$
NEMOs	156±4	2.7±0.2
NEMOb	141±1	2.6±0.1
NEMOf	528±17	3.2±0.3
NEMOc	557±16	3.8±0.4
NEMOm	248±4	3.3±0.1

F

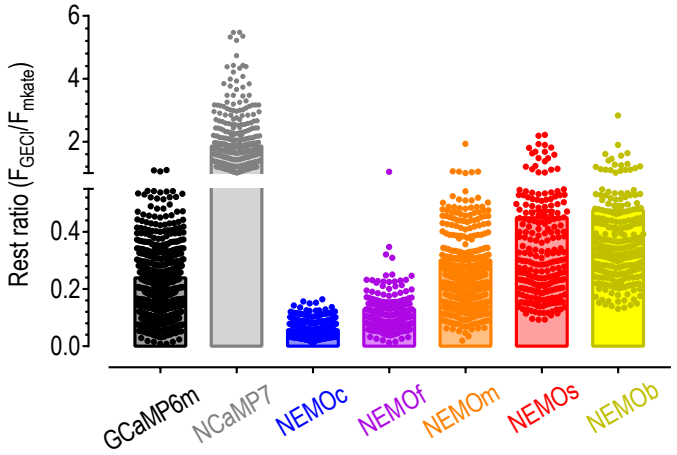

G

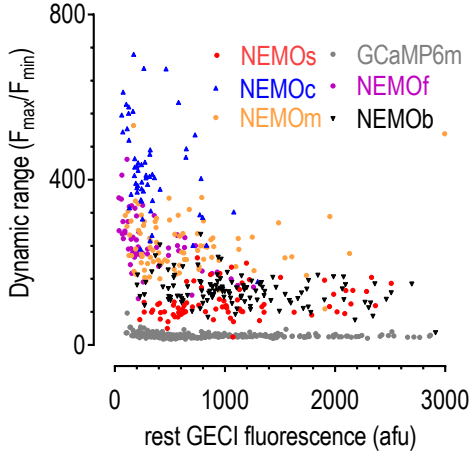

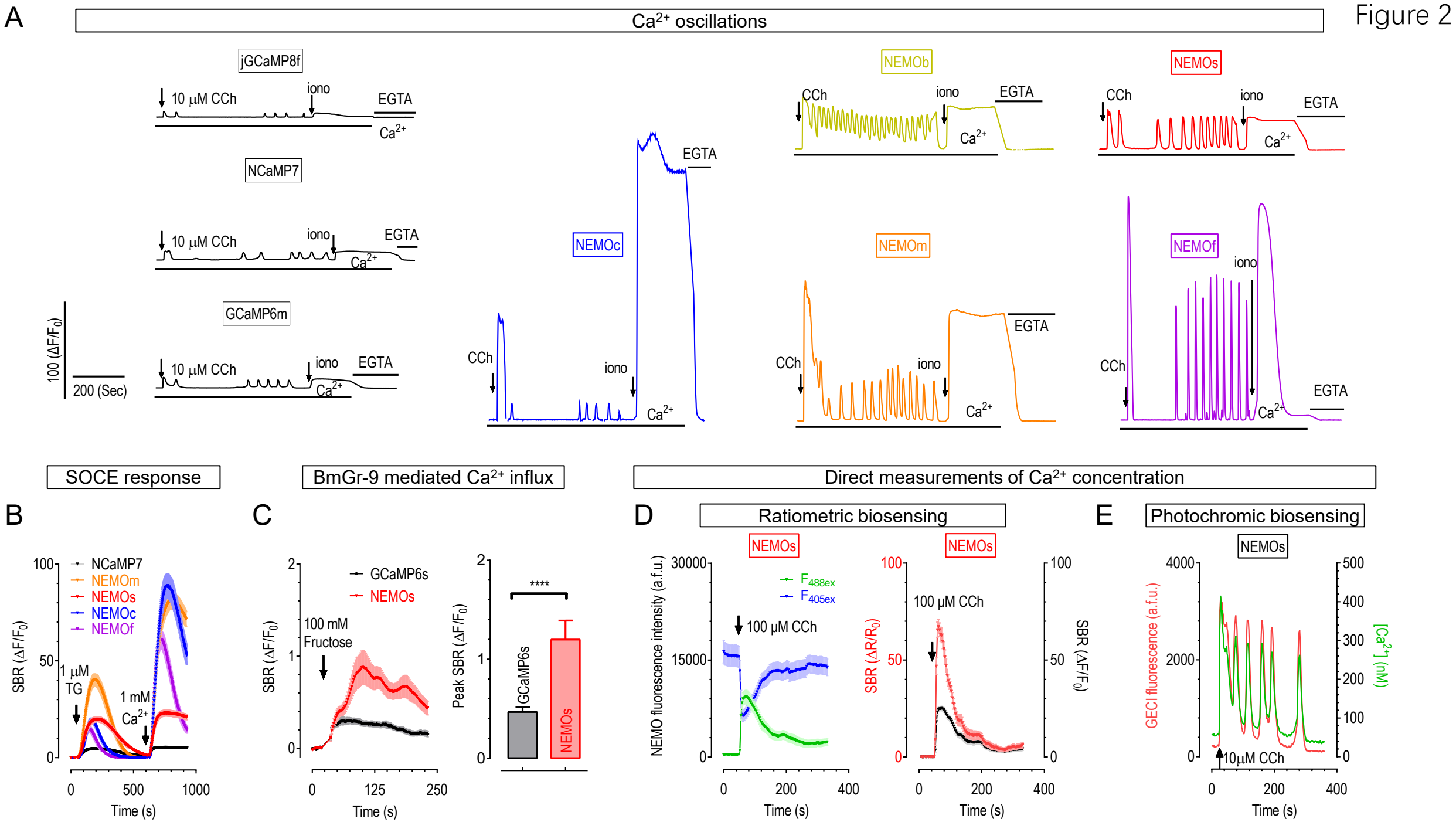

A
Ca2+ oscillations
Figure 2
jGCaMP8f
10 μM CCh
iono
EGTA
Ca2+
NCaMP7
GCaMP6m
100 (ΔF/F0)
200 (Sec)
NEMOc
NEMOb
NEMOs
NEMOm
NEMOf
CCh
SOCE response
BmGr-9 mediated Ca2+ influx
Direct measurements of Ca2+ concentration
B
NCaMP7
NEMOm
NEMOs
NEMOc
NEMOf
1 μM TG
1 mM Ca2+
SBR (ΔF/F0)
Time (s)
C
GCaMP6s
NEMOs
100 mM Fructose
Peak SBR (ΔF/F0)
****
D
Ratiometric biosensing
NEMO fluorescence intensity (a.f.u.)
F488ex
F405ex
100 μM CCh
SBR (ΔR/R0)
E
Photochromic biosensing
GECI fluorescence (a.f.u.)
[Ca2+] (nM)
10μM CCh

Figure 3

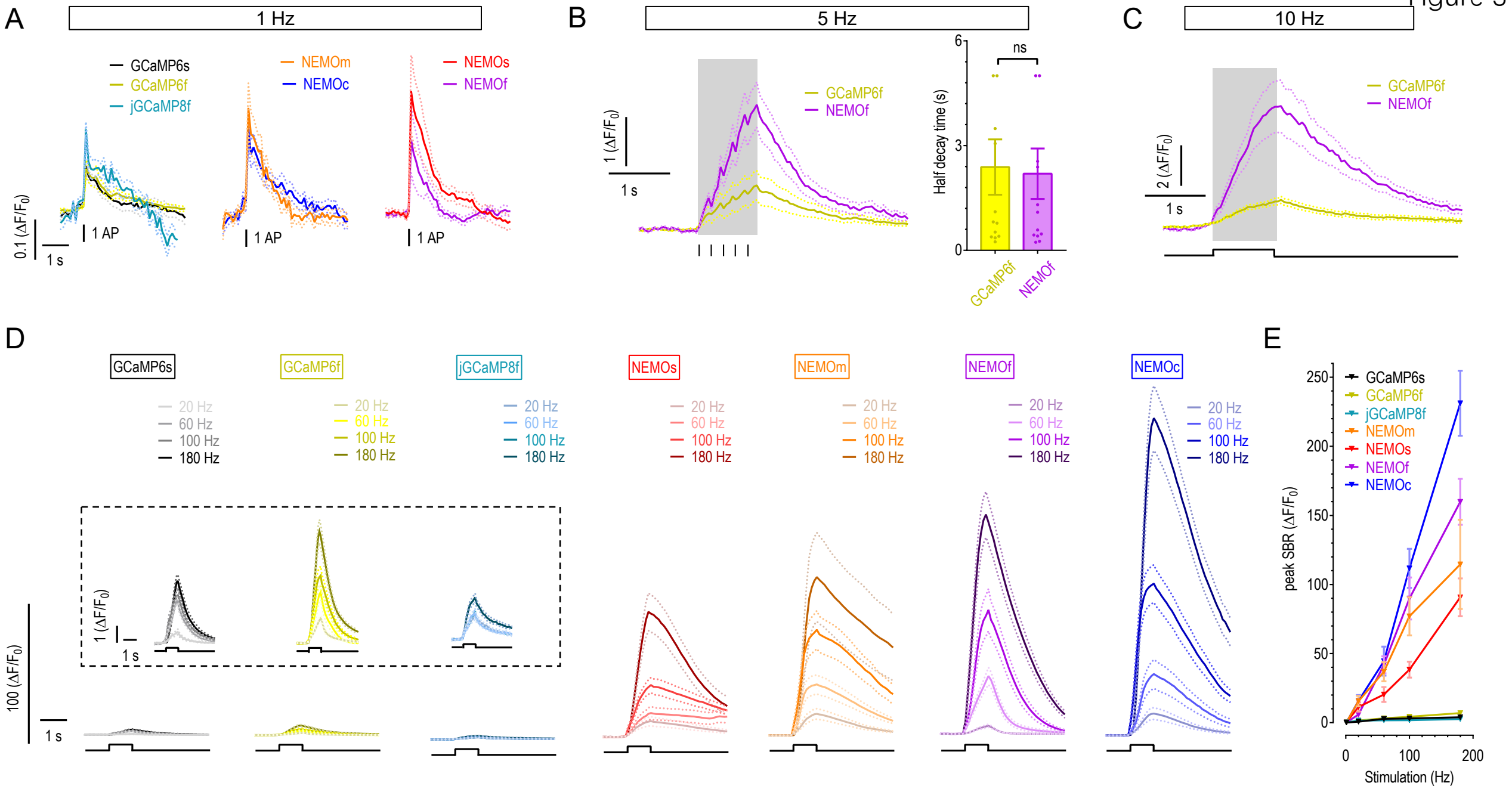
A
1 Hz
GCaMP6s
GCaMP6f
jGCaMP8f
NEMOm
NEMOc
NEMOs
NEMOf
0.1 (ΔF/F0)
1 AP
1 s
B
5 Hz
GCaMP6f
NEMOf
1 (ΔF/F0)
1 s
Half decay time (s)
ns
C
10 Hz
2 (ΔF/F0)
D
20 Hz
60 Hz
100 Hz
180 Hz
100 (ΔF/F0)
E
peak SBR (ΔF/F0)
Stimulation (Hz)

Figure 4

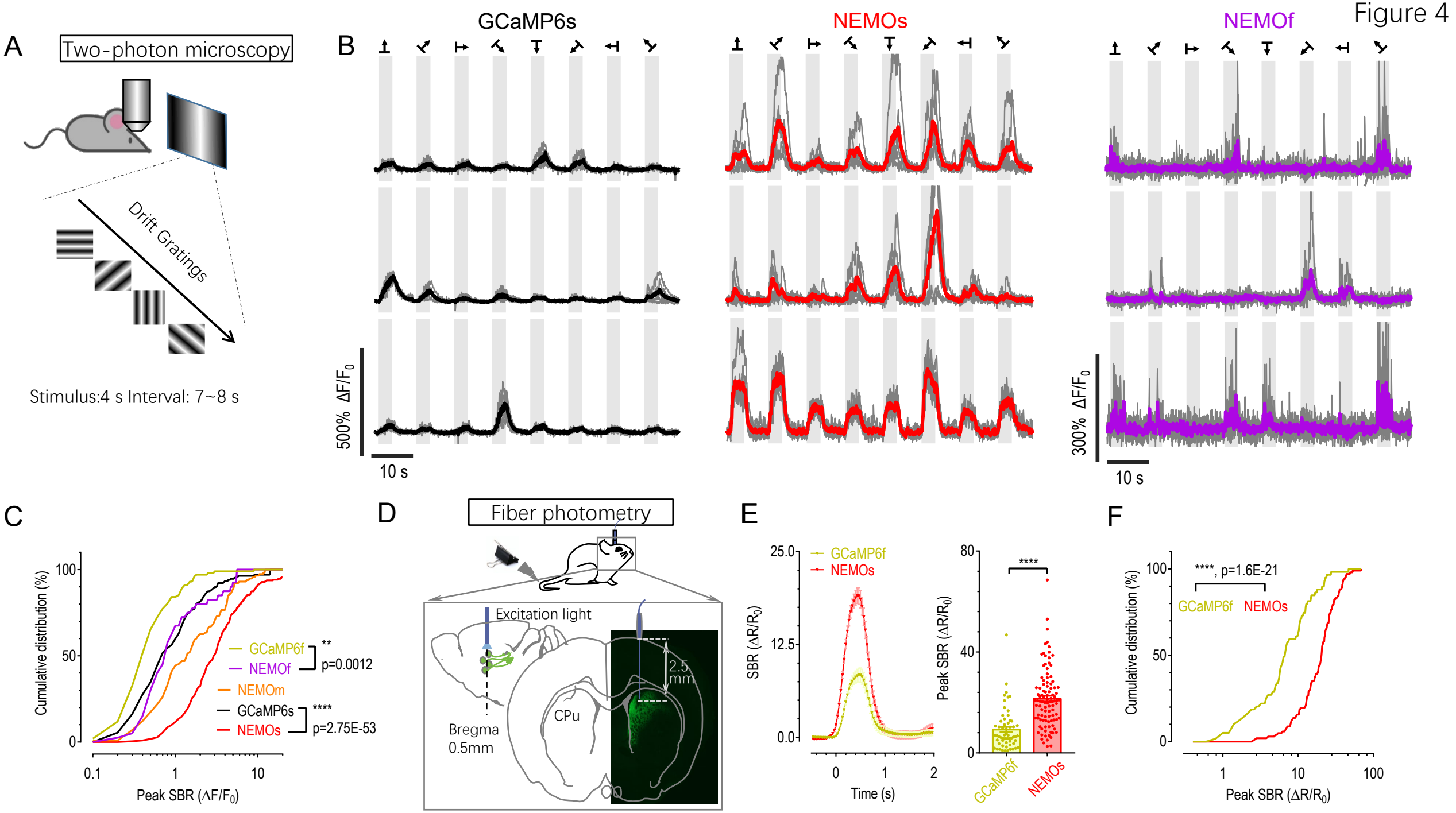
A
Two-photon microscopy
Drift Gratings
Stimulus:4 s Interval: 7~8 s
B
GCaMP6s
NEMOs
NEMOf
500% ΔF/F0
300% ΔF/F0
10 s
C
Cumulative distribution (%)
Peak SBR (ΔF/F0)
GCaMP6f
NEMOf
NEMOm
GCaMP6s
NEMOs
**
p=0.0012
****
p=2.75E-53
D
Fiber photometry
Excitation light
Bregma
0.5mm
CPu
2.5
mm
E
GCaMP6f
NEMOs
SBR (ΔR/R0)
Time (s)
Peak SBR (ΔR/R0)
****
F
****, p=1.6E-21
GCaMP6f
NEMOs
Cumulative distribution (%)
Peak SBR (ΔR/R0)